NASA/TM-20210009682

Melt Infiltration Studies of 2D Tyranno SA3® Ceramic Matrix Composite Preforms With $CrSi_2$ Intermetallic Alloy

S.V. Raj
Glenn Research Center, Cleveland, Ohio

February 2021

NASA STI Program . . . in Profile

Since its founding, NASA has been dedicated to the advancement of aeronautics and space science. The NASA Scientific and Technical Information (STI) Program plays a key part in helping NASA maintain this important role.

The NASA STI Program operates under the auspices of the Agency Chief Information Officer. It collects, organizes, provides for archiving, and disseminates NASA's STI. The NASA STI Program provides access to the NASA Technical Report Server—Registered (NTRS Reg) and NASA Technical Report Server—Public (NTRS) thus providing one of the largest collections of aeronautical and space science STI in the world. Results are published in both non-NASA channels and by NASA in the NASA STI Report Series, which includes the following report types:

- TECHNICAL PUBLICATION. Reports of completed research or a major significant phase of research that present the results of NASA programs and include extensive data or theoretical analysis. Includes compilations of significant scientific and technical data and information deemed to be of continuing reference value. NASA counter-part of peer-reviewed formal professional papers, but has less stringent limitations on manuscript length and extent of graphic presentations.

- TECHNICAL MEMORANDUM. Scientific and technical findings that are preliminary or of specialized interest, e.g., "quick-release" reports, working papers, and bibliographies that contain minimal annotation. Does not contain extensive analysis.

- CONTRACTOR REPORT. Scientific and technical findings by NASA-sponsored contractors and grantees.

- CONFERENCE PUBLICATION. Collected papers from scientific and technical conferences, symposia, seminars, or other meetings sponsored or co-sponsored by NASA.

- SPECIAL PUBLICATION. Scientific, technical, or historical information from NASA programs, projects, and missions, often concerned with subjects having substantial public interest.

- TECHNICAL TRANSLATION. English-language translations of foreign scientific and technical material pertinent to NASA's mission.

For more information about the NASA STI program, see the following:

- Access the NASA STI program home page at http://www.sti.nasa.gov

- E-mail your question to help@sti.nasa.gov

- Fax your question to the NASA STI Information Desk at 757-864-6500

- Telephone the NASA STI Information Desk at 757-864-9658

- Write to:
  NASA STI Program
  Mail Stop 148
  NASA Langley Research Center
  Hampton, VA 23681-2199

NASA/TM-20210009682

Melt Infiltration Studies of 2D Tyranno SA3® Ceramic Matrix Composite Preforms With $CrSi_2$ Intermetallic Alloy

S.V. Raj
Glenn Research Center, Cleveland, Ohio

National Aeronautics and
Space Administration

Glenn Research Center
Cleveland, Ohio 44135

February 2021

Acknowledgments

The author thanks Mr. Robert Angus, Mr. Ray Babuder, and Mr. Gerald Hurd for melt infiltrating the preforms and for other technical assistance. Ms. Joy Buehler prepared the specimens for metallography, and Mr. Terry McCue and Ms. Laura Evans conducted the SEM observations, and their help is gratefully acknowledged. He also thanks Dr. Jeff Eldridge for conducting the Raman spectroscopy analysis. Dr. Roy Sullivan and Mr. Doug Kiser reviewed the manuscript and their valuable comments are gratefully acknowledged. This research was funded by ARMD's Seedling fund program Phases I and II. This paper will published in the Journal of the American Ceramic Society and can be found at https://doi.org/10.1111/jace.17722

Level of Review: This material has been technically reviewed by technical management.

Available from

NASA STI Program
Mail Stop 148
NASA Langley Research Center
Hampton, VA 23681-2199

National Technical Information Service
5285 Port Royal Road
Springfield, VA 22161
703-605-6000

This report is available in electronic form at http://www.sti.nasa.gov/ and http://ntrs.nasa.gov/

Melt Infiltration Studies of 2D Tyranno SA3® Ceramic Matrix Composite Preforms With $CrSi_2$ Intermetallic Alloy

S.V. Raj
National Aeronautics and Space Administration
Glenn Research Center
Cleveland, Ohio 44135

Abstract

This report presents the results of melt-infiltrating 2D Tyranno SA3® fiber woven preforms with molten $CrSi_2$ between 1768 and 1896 K under a vacuum of 1.3×10^{-4} Pa (10^{-6} torr). The infiltration times varied between 1800 and 7200 s, which did not have any significant effect on the volume fraction of voids filled with the metal. Optical and scanning electron microscopy, back scattered electron imaging, energy dispersion spectroscopy, and Raman spectroscopy were used to characterize the infiltrated preforms. A plot of the volume fraction of open voids infiltrated against the absolute melt infiltration temperature showed a sharp peak at 1773 K with almost complete infiltration of the voids at this temperature. The extent of silicide infiltration of the preforms dropped steeply above 1773 K with increasing melt infiltration temperature irrespective of the amount of infiltration time. Above 1805 K, the volume fraction of voids infiltrated with the melt was nearly 0%. It is demonstrated that $CrSi_2$ did not show evidence of a reaction with the SiC fibers. The possibility that a resisting force due to contact angle hysteresis (CAH) may have influenced the diminishing amount of voids filled with increasing temperature above 1773 K was examined. The resistance force was inconsequential since it was estimated to be extremely small. Another possibility that the $CrSi_2$ may have decomposed into Cr(g) and Si(g) in the vacuum melt infiltration furnace appeared to be more plausible based on thermodynamic analyses. An empirical equation is proposed to calculate the amount of remaining charge left to infiltrate the preforms at the infiltration temperature. It is shown that an initial charge of 10 g would rationalize the present observations. While the decomposition of the $CrSi_2$ appeared to mostly explain the present results, some discrepancies were observed, which were inconsistent with the decomposition model.

1.0 Introduction

In an effort to replace Ni-based superalloys in gas turbine engines, a considerable amount of research has been devoted over the last few decades to develop silicon carbide fiber-reinforced ceramic matrix composites (CMCs) for aerospace applications [1,2,3,4,5,6,7,8,9,10,11,12,13,14]. It is expected that several hot section components, such as combustor liners, shrouds, and turbine blades and vanes, made of the lighter weight SiC_m/SiC_f[1] CMCs can operate at higher temperatures and higher pressure ratios with reduced cooling air. As a result, the use of these non-oxide CMCs would increase engine efficiency resulting in lower fuel burn thereby leading to lower CO_2 emissions and significant cost savings in the operation of each aircraft.

However, the low toughness of the SiC_m CMCs limits the design stresses to typically less than the tensile proportional stress of the CMC. This observation is due to the relatively low matrix cracking stress

[1]In this report, SiC_f specifically refers to long fibers in CMCs in contrast to SiC particulates and SiC whiskers used in particulate and whisker-reinforced composites, respectively.

of less than 192 MPa [9,15,16,17,18]. Oxygen ingress through surface-connected cracks can react with the BN coatings on the fibers to form low melting borosilicate glass and critically limit CMC life [9]. Furthermore, the possibility that moisture could enter the CMC through these cracks and attack the fibers and the matrix can also lessen CMC durability. Additionally, unconverted residual Si (i.e., "free Si") in SiC_m/SiC_f CMCs fabricated by Si melt infiltration (MI) significantly limits its use temperature to well below the melting point of Si to ensure that the CMC component has acceptable creep and thermomechanical properties.

For applications as high as 1755 K, the fabrication of CMCs poses a special challenge since conventional Si MI techniques cannot be used for the reasons stated above. In principle, MI with a metal silicide with a higher melting point than pure Si would increase the use temperature of the CMC. However, the thermal expansions of several common silicides are significantly higher than that of SiC, where the extent of deviation increases with increasing temperature [19]. Recently, Raj [19,20] proposed a generalized theoretical approach for designing an engineered matrix (EM) to compensate for the observed differences in the thermal expansion between the silicides and SiC based on the rule of mixtures given by Equation (1):

$$(\Delta L/L_0)_{fiber} = (\Delta L/L_0)_{EM} = V_1(\Delta L/L_0)_1 + V_2(\Delta L/L_0)_2 + V_3(\Delta L/L_0)_3 + \ldots \quad (1)$$

where $(\Delta L/L_0)_{fiber}$ is the thermal strain in the fiber, $(\Delta L/L_0)_{EM}$ is the thermal strain in the EM, $(\Delta L/L_0)_i$ is thermal strain of the i^{th} constituent (i = 1,2,3…n), V_i is the volume fraction of the i^{th} constituent, and $\sum_{i=1}^{n} V_i = 1$. For a three-constituent EM consisting of a silicide, SiC, and Si_3N_4, Equation (1) reduces to

$$(\Delta L/L_0)_{fiber} = (\Delta L/L_0)_{EM} = V_{silicide}(\Delta L/L_0)_{silicide} + V_{SiC}(\Delta L/L_0)_{SiC} + V_{Si3N4}(\Delta L/L_0)_{Si3N4} \quad (2)$$

Additional terms must be included if self-healing and other additives are added to the matrix. Equations (1) and (2) provide a simple way to balance out the thermal expansion differences between the different materials. The validity of this concept was demonstrated in an earlier paper [19].

As noted elsewhere [20], the design of an EM for a CMC with an increased durability for application above the melting point of Si must satisfy certain requirements. These include:

a) A close thermal expansion match between the EM and the SiC_f to minimize the amount of thermal strains developed during thermal fatigue
b) Chemical compatibility and stability of all the constituents
c) The melting points of all the constituents should be above the intended application temperature of the CMC to prevent incipient melting and chemical reaction
d) The presence of ductile second phase particles at the operating temperatures of the CMCs to effectively blunt cracks and prevent their propagation through the matrix
e) Self-healing additives to heal matrix cracks thereby preventing oxygen and H_2O ingress into the CMC through surface-connected cracks and protecting the BN coatings and the SiC_f from reaction

A detailed study of several engineered matrices consisting of high-temperature silicide, SiC, and Si_3N_4 mixtures demonstrated that EMs consisting of 10(vol.%)$CrSi_2$-70%SiC-20%Si_3N_4 ($CrSi_2$-EM) and 10(vol.%)CrMoSi-60%SiC-30%Si_3N_4 (CrMoSi-EM), where CrMoSi is an abbreviation for the Cr-30(at%)Mo-30%Si alloy [21,22,23,24,25], possessed the best combination of bend ductility, bend strength and oxidation properties [20]. The CrMoSi-EM matrix is of particular interest in developing a silicide matrix for applications up to 1773 K.

Figure 1 schematically illustrates the method of fabricating high-temperature engineered ceramic matrix composites (E-CMCs) for applications up to 1773 K. It is envisioned that the CrMoSi-EM containing self-healing additives would be slurry infiltrated into SiC_f woven preform specimens followed by MI with either a binary intermetallic alloy, $CrSi_2$, or a nominal Cr-25 (wt.%)Si[2]. A subsequent suitable heat treatment procedure would be required to ensure that the melt infiltrated silicide alloy bonds the CrMoSi, SiC, and Si_3N_4 particles in the $CrMoSi_2$-EM. Compared to Si MI of woven SiC_f preforms [6,7,8,26], the literature on MI of these preforms with silicides is sparse or non-existent. Earlier research on MI of woven SiC_f preforms with M-Si eutectic alloys [27,28], where M is the metallic element, do not represent true molten silicide infiltration since the eutectic microstructure consists of a large amount of α-Si along with the MSi_2 phase. Since the eutectic temperatures are below that of pure Si, CMCs infiltrated with molten M-Si eutectic alloys are likely to possess lower temperature use capabilities than CMCs infiltrated with molten silicon. In contrast, the silicide alloys used in the present investigation refer to alloy compositions where no free α-Si exists as a thermodynamic equilibrium phase in the microstructure.

The larger objectives of the present investigation were to study the temperature conditions for vacuum melt infiltrating woven Tyranno SA3® (Ube Industries, Ltd., Japan) SiC_f preform specimens with molten $CrSi_2$ and nominal Cr-25%Si. The present paper reports the results of a detailed study conducted to establish the processing conditions for melt infiltrating Tyranno SA3® with molten $CrSi_2$. The results of MI studies of Tyranno SA3® preforms with Cr-25%Si will be reported in a later paper.

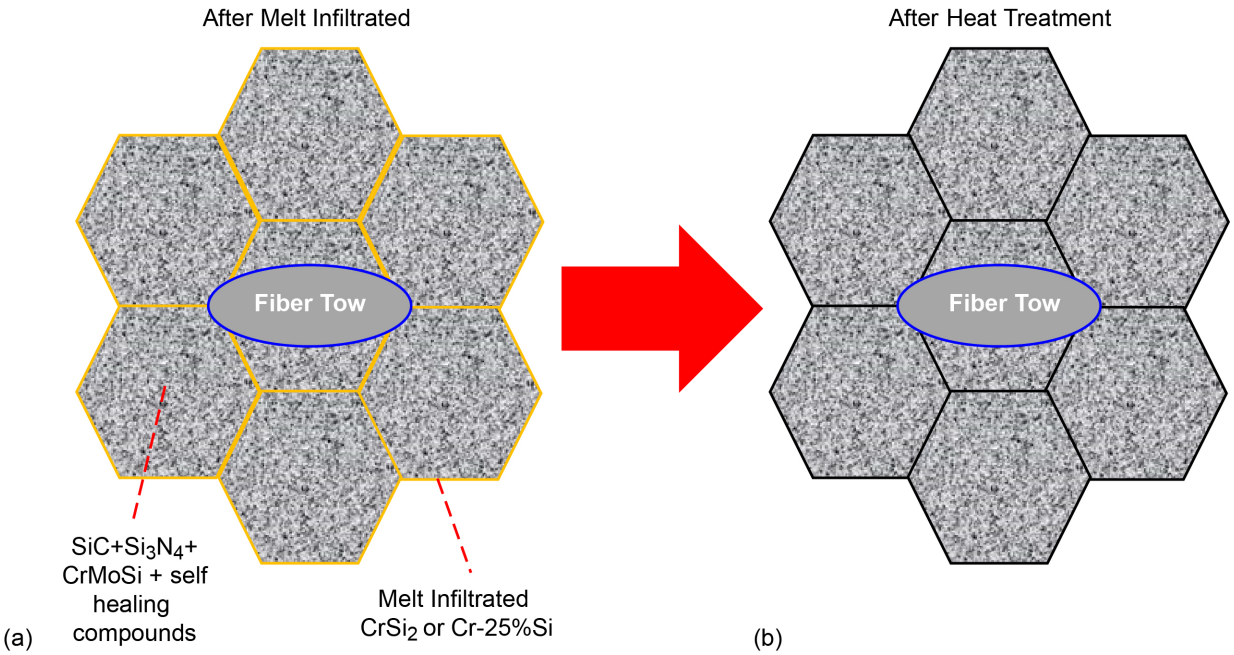

Figure 1.—SiC_f preform slurry infiltrated with a CrMoSi-EM containing self-healing additives. (a) Melt infiltrated with either $CrSi_2$ or Cr-25%Si. (b) Homogenized matrix after homogenizing heat treatment.

[2] Unless otherwise indicated, all compositions are reported in wt.% in this paper.

2.0 Experimental Procedures

2.1 Materials

The 2D Tyranno SA3® fabrics with the fiber tows woven along the 0° and 90° directions were procured from Ube Industries, Japan. The fabrics were fabricated into several panels of dimensions 235 x 160 x 2.1 mm (6-ply) at Hyper-Therm, HTC, Inc., California[3]. A 0.5-μm-thick BN coating deposited on the fibers was overlaid with a thin SiC bond coat by chemical vapor deposition (CVD). Further processing involved chemically vapor infiltrating (CVI) the porosity in the coated preforms with SiC. Thermography inspection of the fabricated panels revealed that they were defect free. The porosity of the specimens determined from geometrical and immersion density measurements revealed that the average volume fraction of open porosity, V_0, in the preforms was 23.8 ± 0.3%. In this case, the density measurements were conducted on four specimens with approximate dimensions 50 x 50 x 2.1 mm sectioned along the length of one of the panels. The dimensions of the specimens used for the MI studies were 10 x 10 x 2.1 mm, which were diamond saw cut from the same panel at low cutting speeds to minimize fiber damage.

The $CrSi_2$ powders (–365 mesh) were procured from Alfa Aesar, Thermo Fisher Scientific. The chemical analyses of the powders were determined by the induction coupled plasma (ICP) technique. The amount of N and O were determined by NSL Analytical Services, Inc., Cleveland, Ohio.

2.2 Melt Infiltration

An examination of the Cr-Si binary phase diagram revealed that $CrSi_2$ melts at 1763 K (1490 °C) [29]. Melt infiltration of the Tyranno SA3® preform specimens was conducted in a high-vacuum graphite melt furnace, where the vacuum levels were typically about 1.3×10^{-4} Pa (10^{-6} torr) at the MI temperature. The preform and a carbon matte were weighed separately before placing the carbon matte on a BN plate followed by placing the preform on top of the matte (Figure 2). The weight of $CrSi_2$ powder varied between 4 and 13 g. The silicide powder was placed on top of the preform as well as around it in a picture frame configuration. Most of the melt infiltration trials were conducted without an external weight, but in a few instances a SiC weight varying between 13.2 and 102 g was placed on top of the silicide powder. In this case, the bottom face of the SiC weight was painted with BN paste. It was noticed that the use of an external weight did not significantly influence the amount of silicide MI into the preform. The BN plate and its contents were introduced into the furnace. The furnace was pumped down to vacuum levels of about 1.3×10^{-4} Pa (10^{-6} torr) before heating the furnace at 600 K/h to the MI temperature. The absolute melt temperatures, T, varied between 1765 and 1900 K for hold times between 1800 and 7200 s for $CrSi_2$. The specimens were furnace cooled to room temperature in a high-vacuum environment after MI.

2.3 Characterization

X-ray microcomputed tomography (μ-CT) scans were performed on a 10 x 10 mm Tyranno SA3® preform sample to obtain a large number of cross-sectional images spaced 10 μm apart, which were stitched together by the instrument's software to enable a 3D visualization of the void morphology in the uninfiltrated preform. Each MI sample was transversally cross-sectioned, and the cross-sections of the cut pieces were mounted and polished for metallographic observations (Figure 3). The arrow in Figure 3 indicates the field of view. Several low magnification digital optical images of the cross-sections of the

[3] Currently, Rolls-Royce Hyper-Therm HTC (RRHT-HTC), Inc.

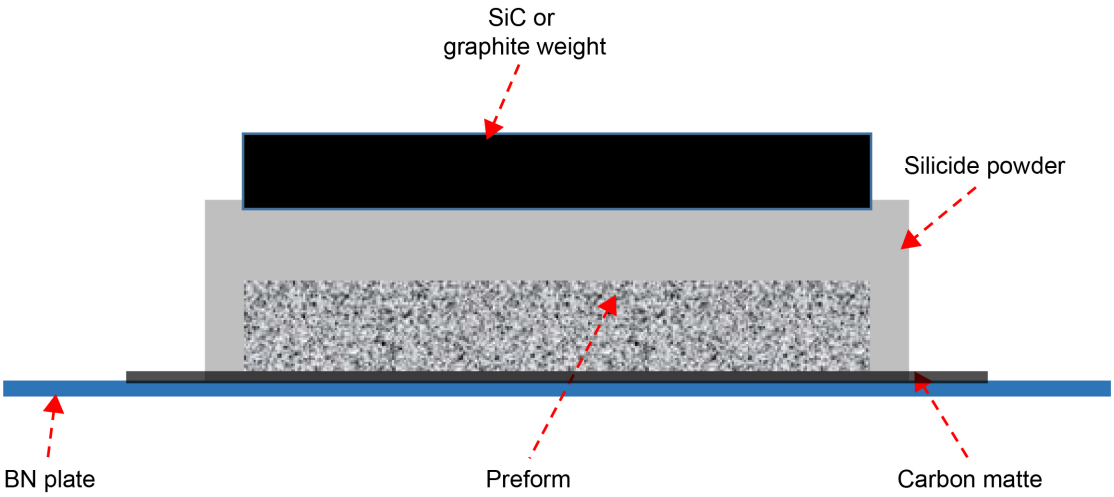

Figure 2.—Setup for melt infiltration of the Tyranno SA3® preform samples with silicide powder.

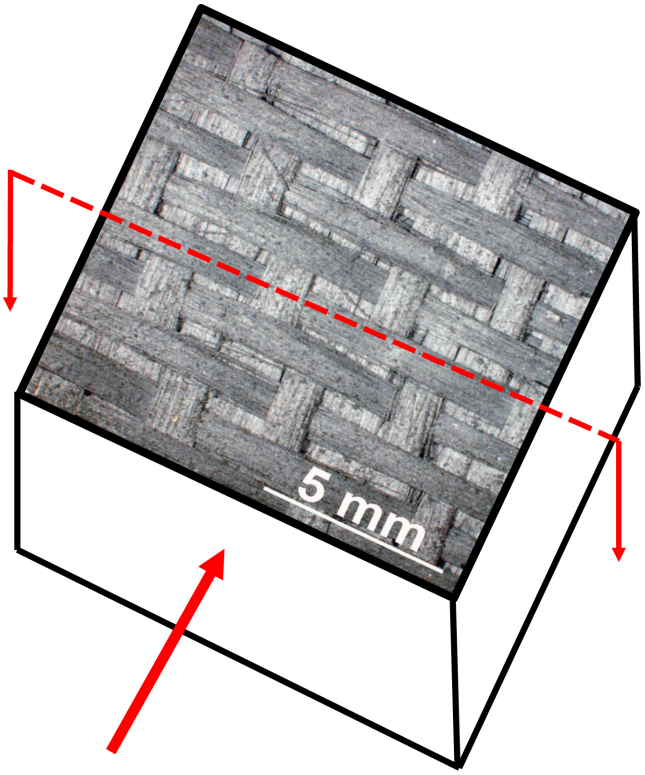

Figure 3.—Relative orientation of the polished cross-section of the specimen used for microstructural observations with respect to entire specimen. Orientation of arrow lies along field of view.

MI samples were obtained at 25x for volume fraction measurements. The volume fractions of the silicide-filled, V_I, and unfilled, V_U, voids were determined by counting the number of grid points that lay on each of these two microstructural features, and dividing them by the total number of grid points using a grid size of 20 x 20 mm in Adobe® Photoshop® CS6 (Adobe Systems, Inc.). The number of images for making these measurements varied between 1 and 6 per MI preform with the total number of grid points selected varying between about 155 and 390. It is important to note that V_U includes both the unfilled open and closed intra-tow and inter-tow voids while V_I is the volume fraction of open voids in the intra-tow and inter-tow regions that were infiltrated by the melt. The average values and the corresponding 95% confidence error bars are reported in this paper. Detailed microstructural observations of the polished cross-sections of the MI specimens were conducted using optical, scanning electron microscopy, back scattered electron (BSE) imaging, and energy dispersive spectroscopy (EDS). Raman spectroscopy was used to determine the amount of free carbon or silicon in the melt infiltrated regions. X-ray diffraction (XRD) analyses were used to verify the compositions of the $CrSi_2$.

3.0 Results

3.1 Characteristics of the Starting Materials

Table 1 shows the actual compositions of $CrSi_2$ powder determined by ICP analysis. An examination of Table 1 reveals that the measured values of Cr and Si in the $CrSi_2$ powder corresponds to 31.4 (at.%)Cr and 66.7(at.%)Si, respectively, with the Si/Cr ratio being 2.1. This ratio is close to the theoretical stoichiometric compositional ratio of 2. The XRD results confirmed the presence of 100(vol.%) of the hexagonal $CrSi_2$ phase. The major substitutional impurities were 0.38% Fe and 0.33%Ti, while the interstitial impurities were 0.196% C, 0.011% N and 0.570% O.

Figure 4(a) and (b) show the μ-computed tomography (μ-CT) scanned image and the optical microstructure of the cross-section of a Tyranno SA3® preform, respectively. The 0° and 90° fiber tows are tightly woven with voids distributed between them. A close examination of Figure 4(b) reveals that the porosity is distributed as intra- and inter-tow voids in the preform. Although most of the inter-tow voids do not appear to be connected to the surface in Figure 4, it is important to note that many of them may be surface connected at other out-of-plane sections. Similarly, not all the intra-tow voids are closed porosity.

TABLE 1.—CHEMICAL COMPOSITION OF THE $CrSi_2$ POWDER, WHERE Cr, Si, AND THE METALLIC IMPURITIES WERE DETERMINED BY INDUCTION COUPLED PLASMA

Cr	46.5
Si	52.4
Al	0.05
C	0.196
Fe	0.38
N	0.011
Ni	0.13
O	0.57
Ti	0.33
Zr	0.05

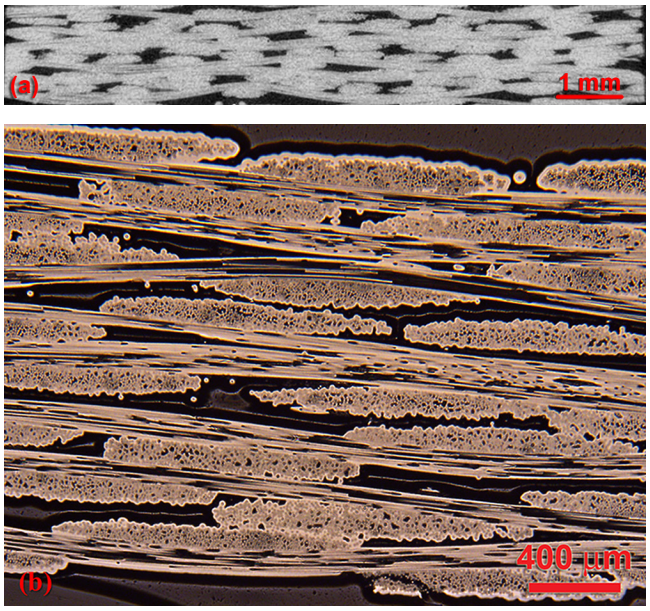

Figure 4.—As-received Tyranno SA3® preform. (a) μ-computed tomography (μ-CT) scan. (b) Optical microstructure of the cross-section. (a) and (b) do not correspond to the same specimen.

3.2 Melt Infiltration With $CrSi_2$

Figure 5(a) and (b) are optical micrographs of a specimen melt infiltrated with $CrSi_2$ at 1803 K for 1800 s. Clearly, a significant number of voids were not infiltrated although the infiltrated $CrSi_2$ is visible in some regions. In this case, the average volume fraction of infiltrated voids was 16.0 ± 3.8%; the corresponding average void volume fraction of uninfiltrated voids was 19.6 ± 4.5%. The molten $CrSi_2$ appears to have separated from the fibers probably due to the shrinkage of the molten metal during solidification. Figure 5(c) shows that the equilibrium contact angle for wetting, θ_e, between the $CrSi_2$ and the SiC_f fibers is $\theta_e > 0°$. Nevertheless, as shown in Figure 5(a) and (b), several areas of the preform were successfully infiltrated with molten $CrSi_2$ thereby suggesting that $CrSi_2$ has partial wettability in Tyranno SA3® preforms. Owing to the relatively large differences in the thermal expansions of $CrSi_2$ and SiC_f [19,20], a large number of cracks were observed in the $CrSi_2$ phase due to the formation of residual tensile stresses during solidification from the melt temperature[4]. Raman spectroscopy of the $CrSi_2$ phase did not reveal the presence of free C and Si, and any free Si that was detected resided in the CVI SiC phase.

Melt infiltration conducted at 1768 K, which is only 5 K above the melting point of $CrSi_2$ [29], for a hold time of 1800 s revealed that the average volume fraction of infiltrated voids was 14.5 ± 2.0% (Figure 6). The corresponding average volume fraction of uninfiltrated voids was 11.2 ± 4.6%. Another 5 K increase in the infiltration temperature to 1773 K for the same hold time resulted in a significant increase in the average volume fraction of infiltrated voids to 25.5 ± 5.3% with the average volume fraction of uninfiltrated voids decreasing to 2.7 ± 1.4% (Figure 7). An infiltration temperature of 1778 K with a hold time of 3600 s decreased the amount of infiltrated voids to an average volume fraction of 20.7 ± 1.6% and a corresponding increase in the average volume fraction of uninfiltrated voids to 14.0 ± 4.9% (Figure 8). The average volume fraction of voids infiltrated was 16.0 ± 3.8% with a corresponding increase in the average

[4]It is important to note that these preforms do not contain the EMs to compensate for the thermal expansion differences between $CrSi_2$ and Tyranno SA3® fibers.

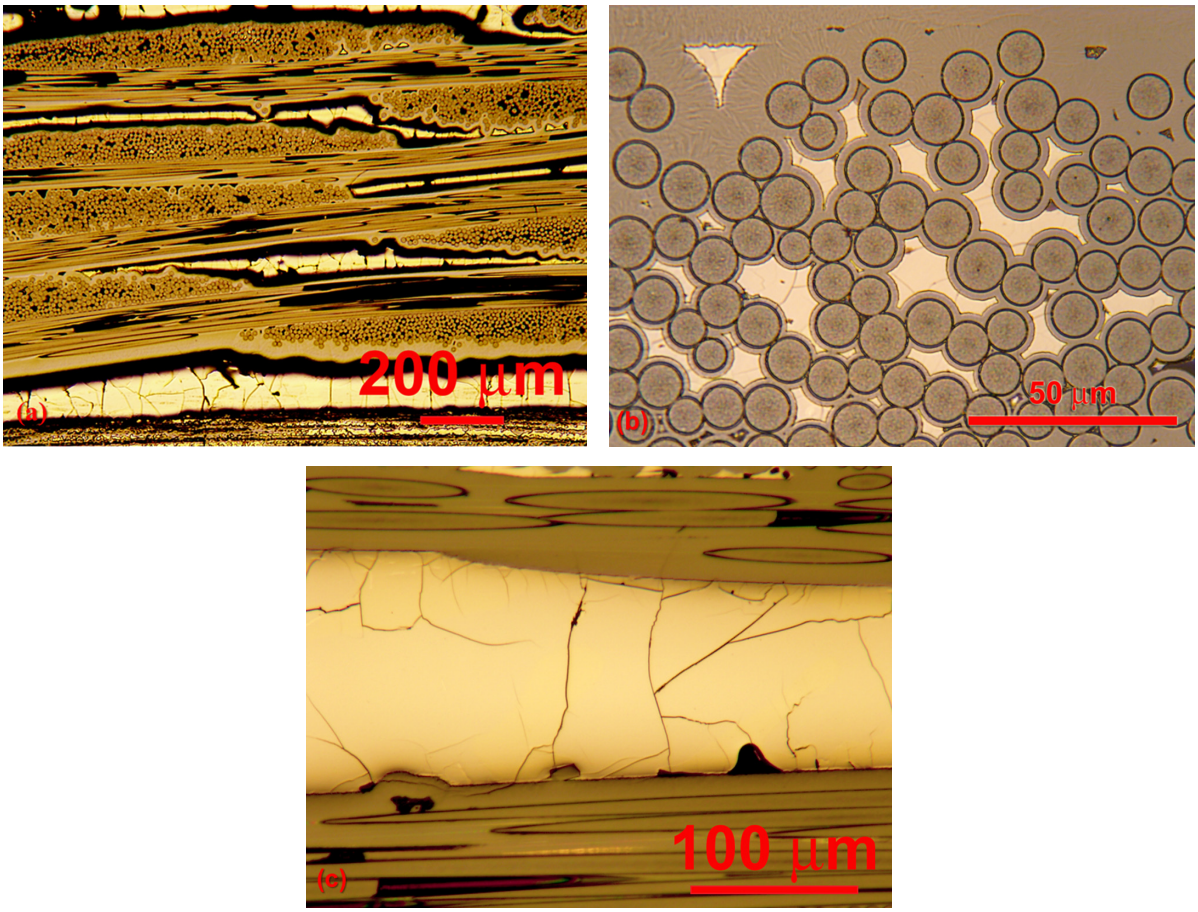

Figure 5.—Optical micrographs of a specimen melt infiltrated with $CrSi_2$ at 1803 K for 1800 s. Cross-sections showing filled and debonded regions of preform. (a) Inter-tow. (b) Intra-tow. (c) High-magnification view of infiltrated $CrSi_2$ demonstrating high wetting contact angle.

volume fraction of uninfiltrated voids to 19.6 ± 4.5% at an infiltration temperature of 1803 K with a hold time of 1800 s (Figure 5(a)). However, an increase in the infiltration temperature by 5 K to 1808 K and a hold time of 1800 s resulted in a sharp drop in the average volume fraction voids infiltrated to about 0.3% with the average volume fraction of uninfiltrated voids being 17.0 ± 1.8%. Between 1823 and 1893 K and for hold times varying between 1800 and 7200 s, the average volume fraction voids infiltrated varied between 0 and 1.2% with the average volume fraction of uninfiltrated voids varying between 28.2 ± 3.0% and 41.7 ± 2.7% (Figure 9).

As discussed earlier, $CrSi_2$ exhibits $\theta_e > 0°$ with the SiC_f fiber surfaces (Figure 5(c)). Although there appears to be no data on the value of θ_e for $CrSi_2$ on a SiC surface, Champion et al. [30] have reported that it is less than 40° for Cr_3Si_2 (Cr_5Si_3)[5] alloy and Si at 1733 and 1723 K, respectively. It is important to note that the magnitude of θ_e will be influenced by the presence of a SiO_2 layer on the SiC_f tows with values of $\theta_e \sim 90°$ for Si on SiO_2 [31]. In nonreactive molten metal-ceramic substrate systems, good wettability is attained when $0° < \theta_e < 90°$ with typical values of $\theta_e \sim 40\text{-}50°$ for molten Si on a SiC substrate [28,31,32]. The melt is fluid when $\theta_e = 0$ and less fluid when $\theta_e = 90°$. It has been demonstrated that increasing the Cr content of molten Cu-Cr and Cu-Ni alloys, significantly lowers the magnitudes of

[5] Champion et al. [30] identify the alloy as Cr_3Si_2. However, the binary Cr-Si phase diagram [29] does not show the existence of this phase. Since the Cr:Si for Cr_3Si_2 is 1.5, it is possible that the phase referred to in Ref. [30] was misidentified and actually refers to the Cr_5Si_3 phase in the phase diagram for which Cr:Si is about 1.67.

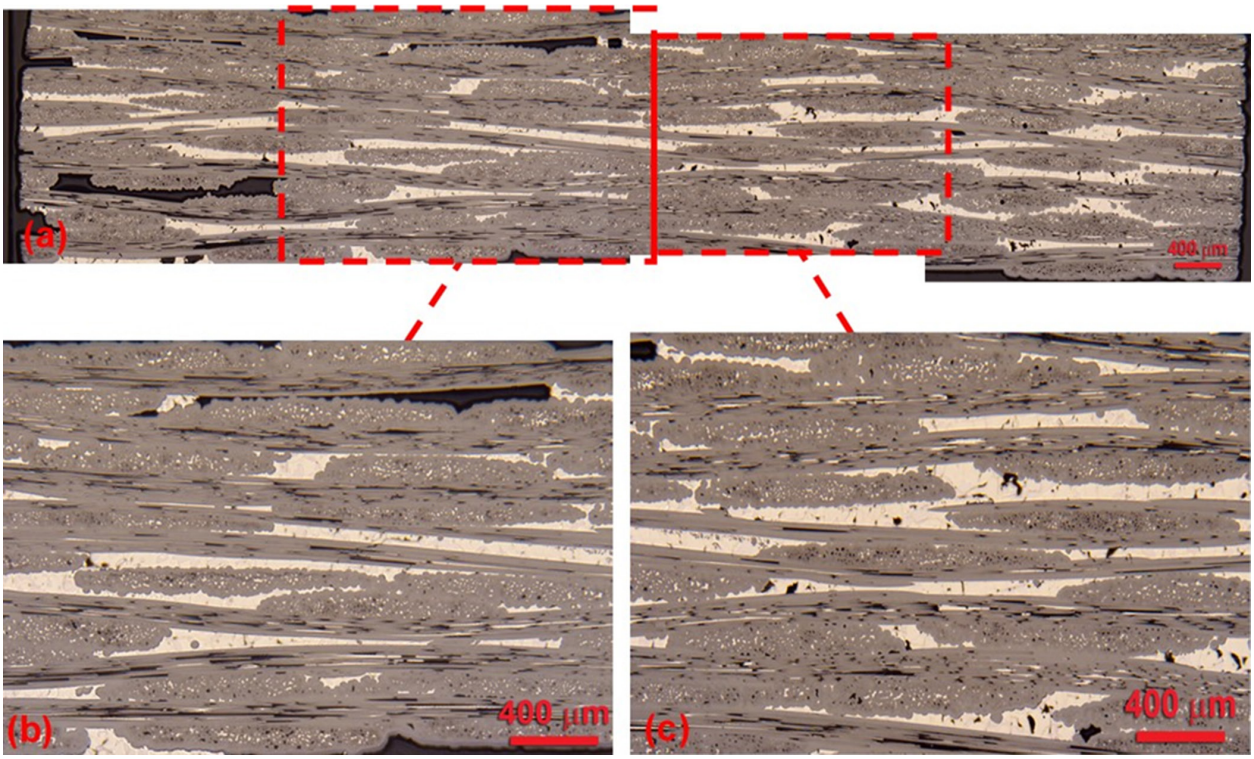

Figure 6.—Optical micrographs of the cross-section of a specimen melt infiltrated with $CrSi_2$ at 1,768 K for 1,800 s. (a) Full specimen. (b) Close-up of left side of (a). (c) Close-up of right side of (a).

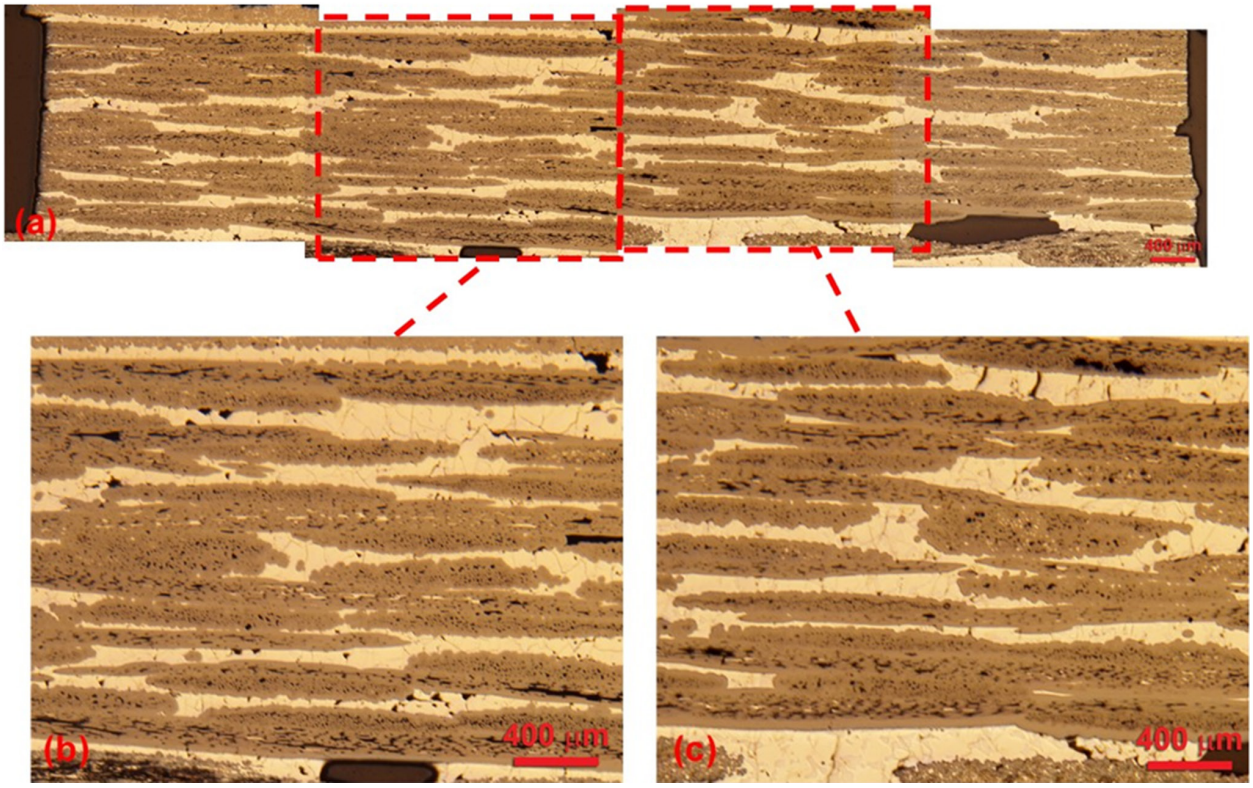

Figure 7.—Optical micrographs of the cross-section of a specimen melt infiltrated with $CrSi_2$ at 1773 K for 1800 s. (a) Full specimen. (b) Close-up of left side of (a). (c) Close-up of right side of (a).

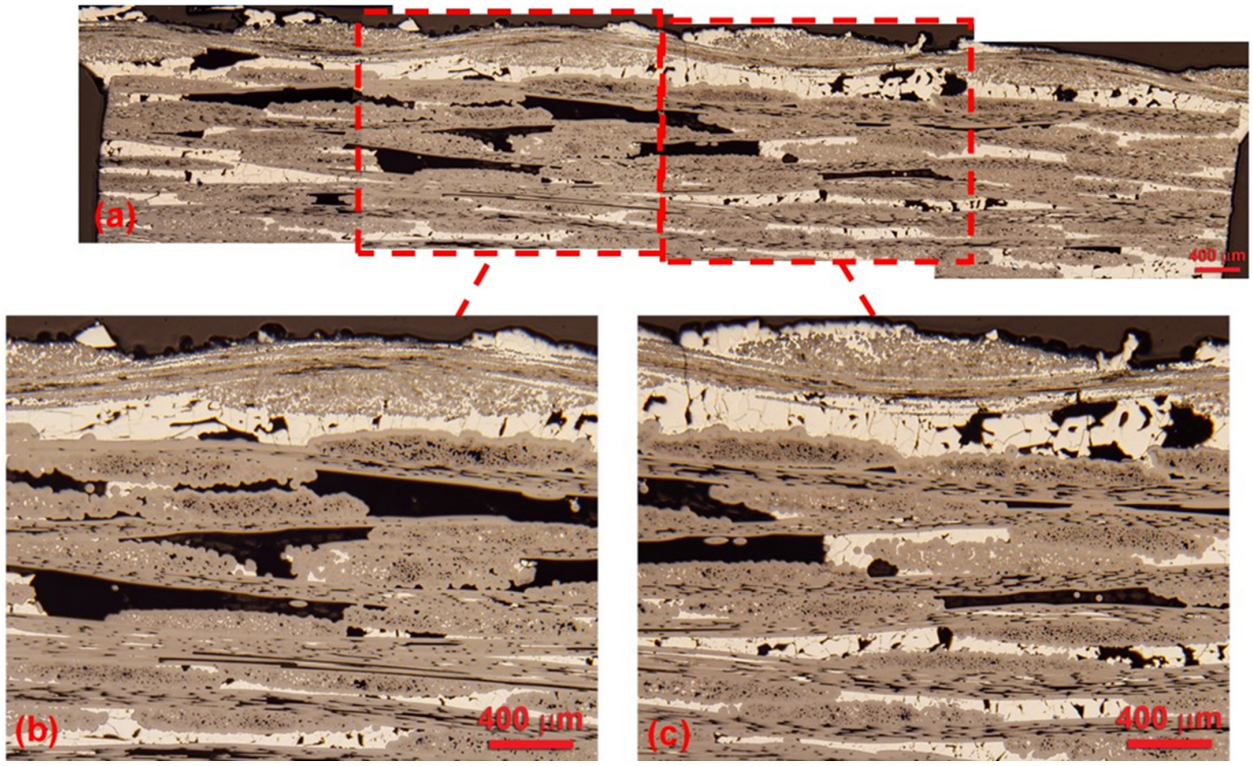

Figure 8.—Optical micrographs of the cross-section of a specimen melt infiltrated with $CrSi_2$ at 1778 K for 3600 s. (a) Full specimen. (b) Close-up of left side of (a). (c) Close-up of right side of (a).

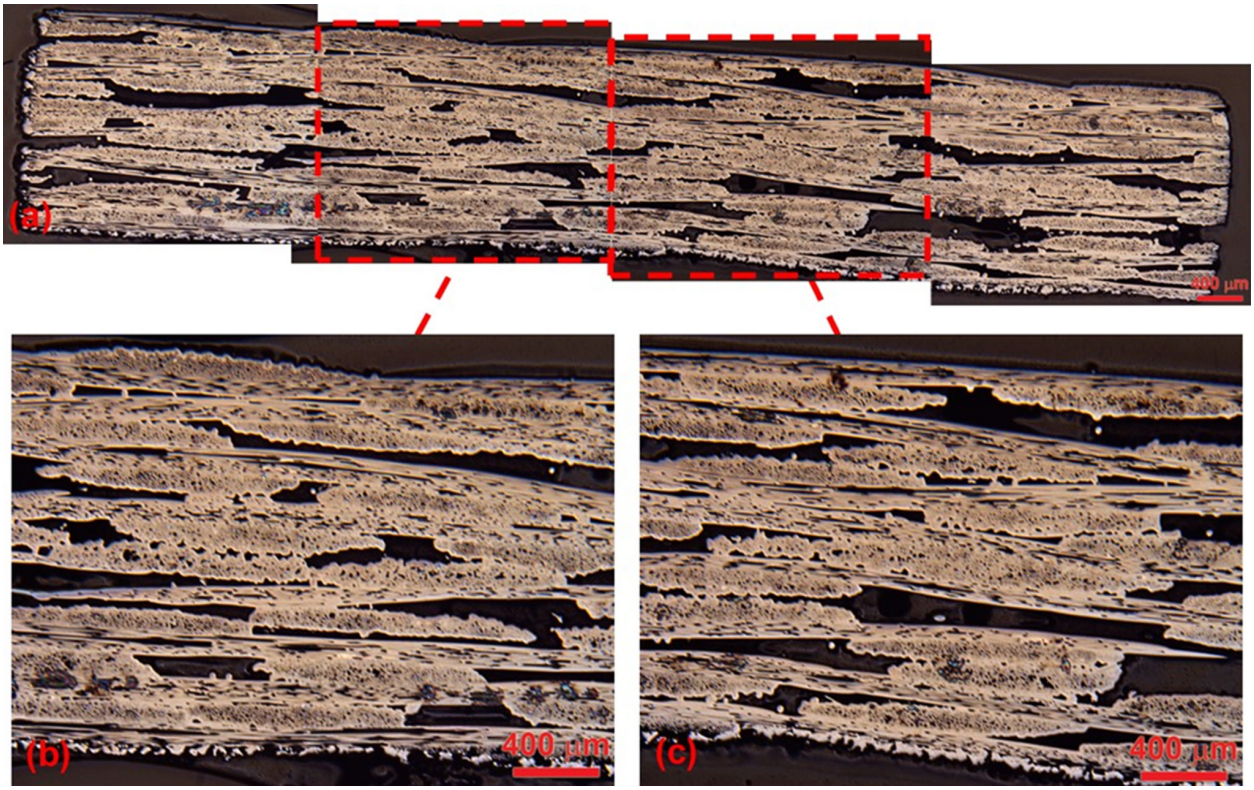

Figure 9.—Optical micrographs of the cross-section of a specimen melt infiltrated with $CrSi_2$ at 1823 K for 7200 s. (a) Full specimen. (b) Close-up of left side of (a). (c) Close-up of right side of (a).

θ_e on SiC substrates with a corresponding increase in the wettability of the alloy [33]. Therefore, it is reasonable to assume that $\theta_e < 90°$ for molten $CrSi_2$ on the surfaces of Tyranno SA3® fibers in the preforms infiltrated in this investigation thereby suggesting good wettability. However, the absence of any significant infiltration of the molten metal at high temperatures as shown in Figure 8 to Figure 10 indicates that other factors influence the conditions under which the molten $CrSi_2$ metal will successfully infiltrate the Tyranno SA3® preforms even if $\theta_e < 90°$.

Figure 10 shows the variation of V_I and V_U as a function of T, where the error bars represent the 95% confidence limits. The vertical broken line represents the absolute melting temperature for $CrSi_2$ [29]. The lower horizontal broken line represents the volume fraction of open voids in the as-received Tyranno SA3® preform measured by the immersion density method. The upper horizontal broken line is the average total void volume fraction in the preform determined by averaging the summation, $V_I + V_U$, where the gray band about this line defines the 95% confidence limits. The sum $V_I + V_U$ varied between 28 and 40%. The average value of $V_0 = 23.8 \pm 0.3\%$ in the uninfiltrated preforms is shown in Figure 10 as a horizontal black broken line[6]. It is noted that the actual magnitude of V_0 in individual preform specimens could be higher or lower than this value.

A close examination of Figure 10 reveals that the temperature dependence of V_I increases steeply as the infiltration temperature increases by just 5 K from 1768 K (Figure 6(a) to (c)) to 1773 K (Figure 6(a) to (c)), and falls steeply as temperature increases by another 5 K to 1778 K (Figure 8(a) to (c)), where the corresponding values of V_I are 14.5 ± 2.0, 25.4 ± 5.3 and $20.7 \pm 1.6\%$, respectively. An inverse but not identical profile is observed for the temperature dependence of V_U. The sharp peak observed in the V_I-T curve indicates that these results may not be easily reproducible. This hypothesis was confirmed by melt infiltrating a second specimen at 1778 K for which the measured value of V_I was $0.7 \pm 0.4\%$[7]. The magnitude of V_I decreased to $16.0 \pm 3.4\%$ with a further increase in the MI temperature by 5 K to 1803 K. However, the magnitude of $V_I \approx 6.4 \pm 2.1\%$ was for another specimen melt infiltrated at 1803 K. Above 1803 K, the measured values of V_I generally varied between 0 to 0.3% (Figure 9(a) to (c)). Once again, the results were not reproducible as expected from the sharp profile shown in Figure 10. Despite the difficulty in reproducing the data, it is clear from Figure 10 that the MI temperature range lies between 1770 and 1800 K to achieve at least 5% infiltration of the preforms. The effect of hold time at the MI temperature did not appear to consistently influence the magnitude of V_I (Figure 11). This observation suggests that the infiltration velocities of the liquid metal were sufficiently fast to ensure that the preforms were infiltrated before the minimum experimental hold time of 1800 s.

[6] It should be noted that the immersion density measurement of V_0 is dependent on the ability of the liquid medium to infiltrate all the open voids. This may not always be the case if residual air is present or the surface tension of the liquid prevents the fluid surface from infiltrating some of the voids. Thus, V_0 may be lower than $V_I + V_U$. It is also important to note that V_0, and $V_I + V_U$, were determined by two different methods. As a result, $V_I + V_U$ are expected to be more sensitive to local variations in the void volume fraction than V_0.

[7] It is noted that the hold times for the first and second specimens at 1778 K were 3600 and 1800 s, respectively. Despite the fact that the amount of infiltration was significantly higher for the former than for the latter specimen, these differences in hold times are not significant.

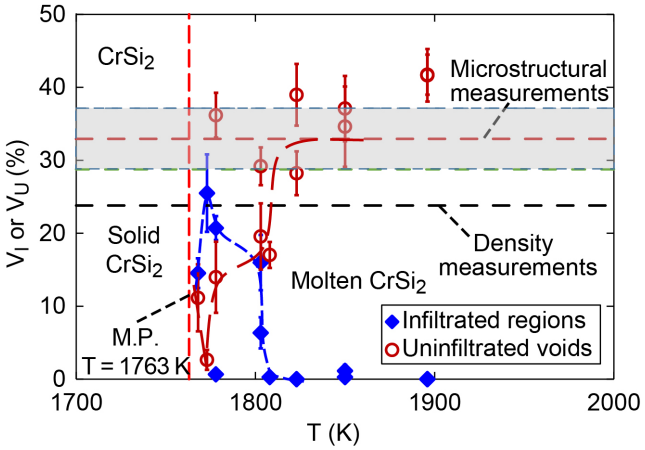

Figure 10.—Average volume fractions of $CrSi_2$-infiltrated, V_I, and uninfiltrated, V_U, regions in Tyranno SA3® specimens as a function of absolute melting temperature T. Filled diamond and open circle symbols represent V_I and V_U, respectively, with error bars representing 95%confidence limits. Vertical broken line shows absolute melting point for $CrSi_2$ [29]. Bottom horizontal broken line shows average value of open voids in uninfiltrated CMC measured by immersion density method. Top horizontal broken line shows average total void volume fraction of voids given by sum, $V_I + V_U$, where gray region represents 95% confidence limits about this line.

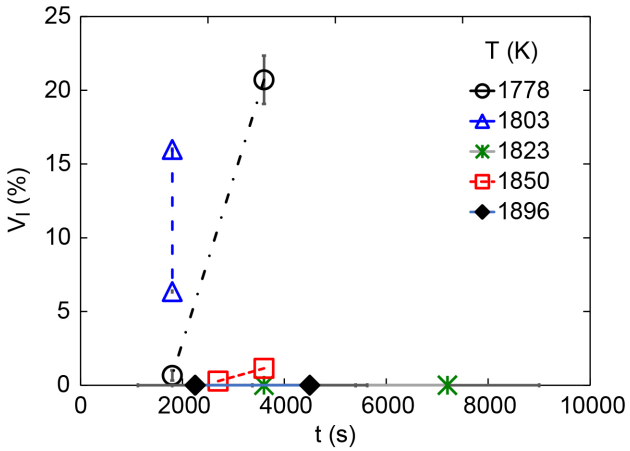

Figure 11.—Variation of average volume fraction of $CrSi_2$-infiltrated V_I against hold time t at different melt infiltration temperatures T.

3.3 Reaction Studies

Several Raman spectral point analyses of the infiltrated $CrSi_2$ phase in a preform melt infiltrated at 1803 K for 1800 s confirmed the absence of free Si. Low magnification optical microstructures revealed that the molten $CrSi_2$ had not reacted with the CVI SiC or the BN-coated SiC_f tows (Figure 5 to Figure 8). These observations were confirmed by high magnification BSE microstructures of the $CrSi_2$-CVI SiC interfaces as shown in Figure 12, where the EDS spectrum from region A in the $CrSi_2$ phase shows strong Cr and Si peaks. Similarly, Figure 13(a) and (b) and the EDS spectra from regions A and B in Figure 13(b) demonstrate that the molten $CrSi_2$ had not reacted with the preform during MI at 1823 K for 1800 s.

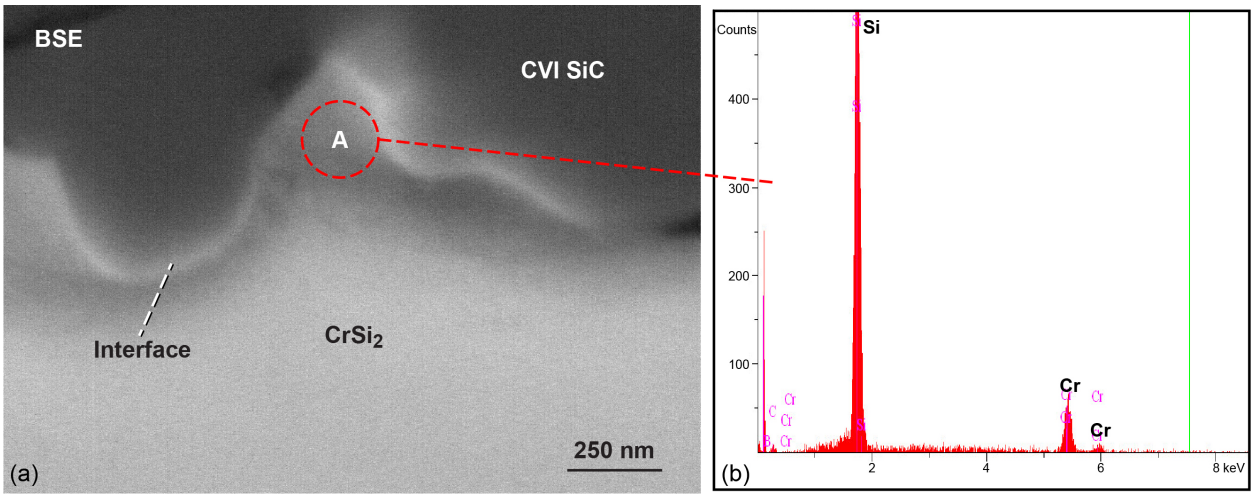

Figure 12.—$CrSi_2$-chemical vapor infiltrated (CVI) SiC interface in a specimen melt infiltrated at 1803 K for 1800 s and sputter coated with a carbon coating. (a) High magnification back scattered electron view demonstrating that there was no reaction between molten $CrSi_2$ and CVI SiC. (b) Energy dispersive spectroscopy spectrum of region A in $CrSi_2$ confirms only presence of Cr and Si peaks.

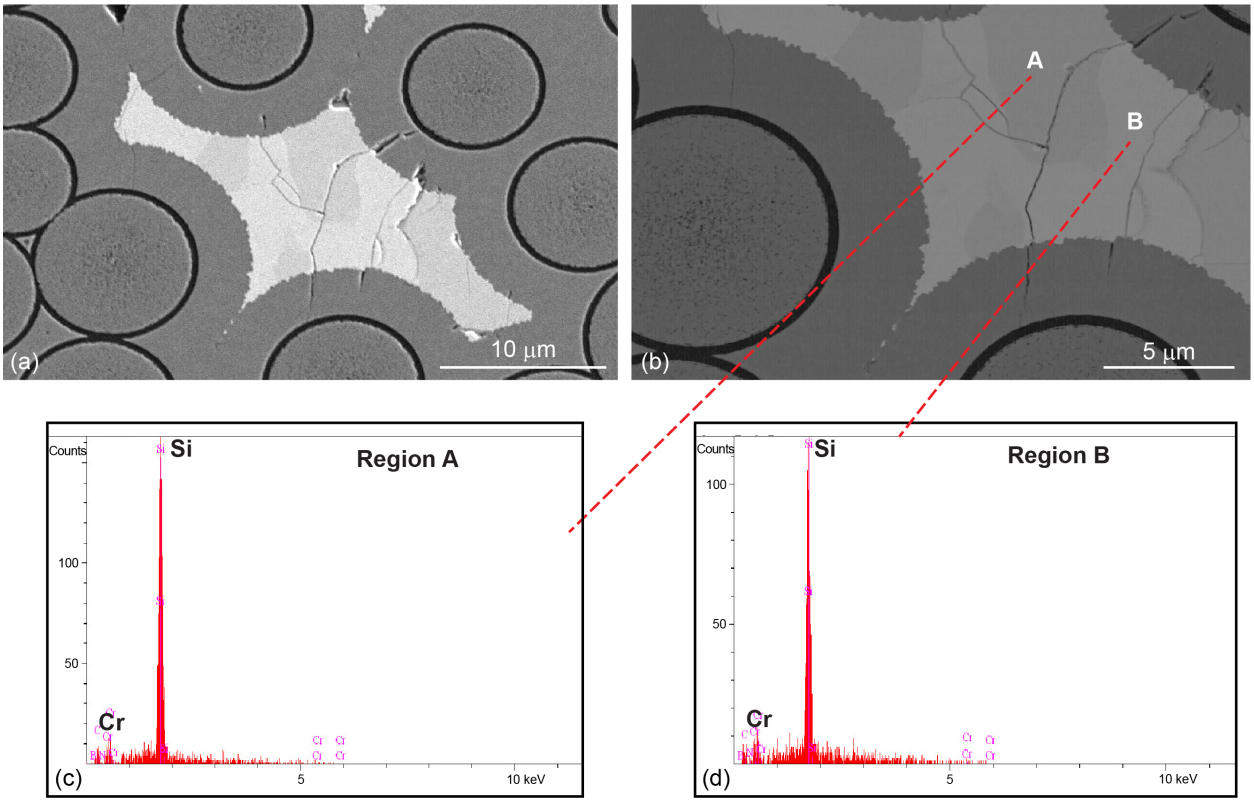

Figure 13.—Interior region of $CrSi_2$ melt infiltrated Tyranno SA3® preform infiltrated at 1823 K for 1800 s. (a) Scanning electron microscope image. (b) Back scattered electron image showing corresponding electron disperse spectra from (c) region A and (d) region B demonstrating that the molten $CrSi_2$ did not react with preform.

4.0 Discussion

The present investigation has demonstrated that it is possible to nearly completely infiltrate Tyranno SA3® preforms with molten $CrSi_2$ without reaction although the results are difficult to reproduce. The shape of the infiltration curve in Figure 10 involving the initial increase in V_I with increasing temperature until 1773 K followed by a decrease to 0% above 1808 K is curious and unusual. The increase in V_I with increasing temperature can be qualitatively attributed to a decrease in the dynamic viscosity, μ, and a corresponding increase in metal fluidity, $\phi = 1/\mu$ [34,35]. However, the subsequent decrease in V_I with increasing temperature is puzzling. The exact reason for this observation is unclear at present. However, two probable causes are considered in this paper, which may partly or fully explain this decrease. First, the possible role of contact angle hysteresis (CAH), θ_H, of the molten droplets [36] on resisting the MI of the preforms is discussed. Second, the effect of the high-vacuum environment in aiding the decomposition of the molten $CrSi_2$ at high temperatures is also examined.

4.1 Role of Contact Angle Hysteresis on Melt Infiltration

Several investigators have investigated the MI of preforms with molten metal and proposed quantitative models based on either the Darcy or the Hagen-Poiseuille equation to predict the depth of penetration of the molten metal into the preforms [28,30,31,32,33,37,38,39,40,41,42,43]. In most instances, these models have assumed that capillary flow of the molten metal under a differential pressure, ΔP, readily occurs when the wettability condition $\theta_e < 90°$ is satisfied. An implicit assumption in these models is that there is no CAH. There is now a considerable body of evidence that demonstrates the flow of a fluid may not occur on an inclined or a vertical surface if the capillary force due to a large CAH exceeds the gravitational force acting on the droplets [36,44,45,46,47,48,49,50,51]. These investigations have demonstrated that the advancing contact angle, θ_a, and the receding contact angle, θ_r, of a fluid droplet can be different from θ_e thereby leading to the observation of a CAH, which resists the gravitational force acting on the droplets. Different methods are used to calculate θ_H including $\theta_H = \theta_a - \theta_r$ and $\Delta\cos\theta_H = \cos\theta_r - \cos\theta_a$, where the latter relationship is related to the capillary force, F_{Cl} [36,44,45]. Several investigators define $\theta_a = \theta_e + \frac{\Delta\theta_H}{2}$ and $\theta_r = \theta_e - \frac{\Delta\theta_H}{2}$ [44,46]. The magnitude of F_{Cl} is given by [46]

$$F_{Cl} = 2\sigma R_0(\cos\theta_r - \cos\theta_a) = 2\sigma R_0 \Delta\cos\theta_H \quad (3)$$

where σ is the surface tension of the molten metal and $R_0 = \frac{d_v}{2}$ is the radius of the droplet (Figure 14).

Figure 14 shows the schematic cross-section of a 0/90° of a 4-ply SiC_f/SiC_f preform with a center-to-center fiber spacing, d_f, pore size at the preform free surface, d_V, in contact with a volume of the nonreactive molten metal on its top surface. The fluidity of the molten $CrSi_2$ increases with increasing temperature due to a corresponding decrease in its viscosity. This increase in melt fluidity results in an increase in the magnitude of its surface velocity, U_t, parallel to the top surface of the preform due to the resulting volume expansion of the molten metal as it spreads on preform surface. The macroscopic infiltration velocity, U_F, of the molten metal is in the z-direction. If the molten droplets have CAH as shown in Figure 14, then the gravitational force, mg, will be resisted by F_{Cl}, where m is the mass of the paraboloidal molten droplet and g is the acceleration due to gravity. Thus, the local force balance assuming an applied pressure, P_a, on the molten metal [45,46,52,53,54,55]

$$m\frac{dU_F}{dt} = mg + \pi R_0^2 P_a - 2\sigma R_0 \Delta\cos\theta_H \tag{4}$$

The average equilibrium volume of the paraboloidal droplet is $V_e = \frac{\pi}{2}R_0^2 H_0$, where H_0 is maximum thickness of the droplet, so that with $\theta_e = \tan^{-1}\left(\frac{2H_0}{R_0}\right)$, the magnitudes of H_0 and R_0 are given by [56][8]

$$R_0 = \frac{d_v}{2} = \left(\frac{4V_e}{\pi\tan\theta_e}\right)^{1/3} \tag{5a}$$

$$H_0 = \frac{\tan\theta_e}{2}\left(\frac{4V_e}{\pi\tan\theta_e}\right)^{1/3} = \frac{\tan\theta_e}{2}\left(\frac{d_v}{2}\right) \tag{5b}$$

Clearly, the magnitudes of H_0 and R_0 are determined by the magnitudes of d_v and θ_e. Thus, with $m = \frac{1}{2}\pi R_0^2 H_0 \rho$, where ρ is the density of the molten metal, Equation (4) becomes

$$\rho\frac{dU_F}{dt} = \rho g + \frac{2P_a}{H_0} - \frac{4\sigma}{\pi H_0 R_0}\Delta\cos\theta_H \tag{6}$$

For immobile droplets, $U_F \leq 0$, so that from Equations (5a), (5b), and (6), and rearranging the terms, we have

$$2\sigma\,\Delta\cos\theta_H \geq \frac{\pi d_v^2}{16}\left(\rho g + \frac{2P_a}{H_0}\right) \tag{7}$$

In the specific case of vacuum MI, $P_a = 0$, and Equation (7) reduces to

$$2\sigma\,\Delta\cos\theta_H \geq \frac{\pi\rho g d_v^2}{16} \tag{8}$$

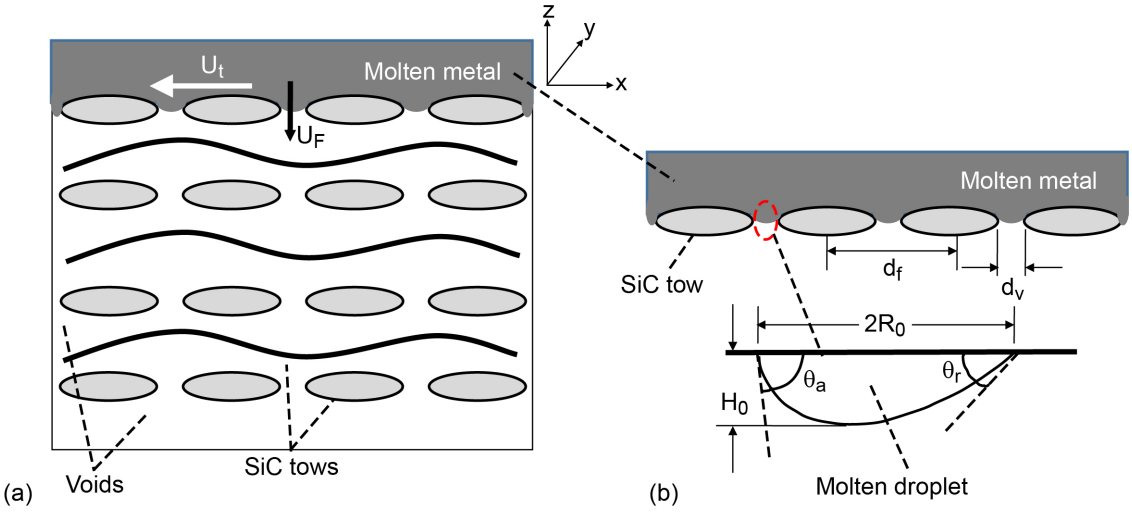

Figure 14.—Cross-section of 0/90° of a 4-ply SiC_f/SiC_f preform (a) showing molten metal flowing at outer surface with velocity, U_t, and macroscopic infiltration velocity, U_F. (b) Infiltrated preform outer surface close-up showing average void diameter is d_v, Molten paraboloid droplet with an advancing contact angle, θ_a, and receding contact angle, θ_r. Surfaces of SiC_f fibers in preform will experience force opposing gravitational force due to contact angle hysteresis, thereby resisting infiltration of preform.

[8] Equations (5a) and (5b) are generalized representations since the corresponding equations shown in Reference 56 assume θ_e is small so that $\tan\theta_e \approx \theta_e$.

Equations (7) and (8) define the conditions under which the molten metal will not infiltrate the preform under an applied pressure and in a high vacuum, respectively. Using a value of $\rho = 5020$ kg/m^3 for $CrSi_2$ [57], g = 9.80 m/s^2 and $d_v \approx 115$ to170 μm for Tyranno SA3®, the magnitude of $2\sigma \Delta\cos\theta_H \geq$ 1.3 to 2.3×10^{-4} N/m under high-vacuum MI conditions. The corresponding magnitude of F_{Cl} from Equation (3) varies between 0.007 and 0.023 μN. This is an extremely small resistance force, and clearly, the incomplete or non-infiltration of the preforms observed in Figure 8 to Figure 10 cannot be attributed to the effect of CAH. This deduction is consistent with the fact that almost complete infiltration was observed in one specimen at 1773 K (Figure 7).

4.2 Decomposition of $CrSi_2$

In the absence of a significant CAH resistance force being a possible cause for the incomplete or non-infiltration of the preforms observed above 1773 K in Figure 8 to Figure 10, the possibility that a substantial amount of the initial $CrSi_2$ charge had vaporized after melting at high temperatures in the high-vacuum environment must be examined. The decomposition of the molten $CrSi_2$ is represented as

$$CrSi_2\ (l) \rightarrow Cr\ (g) + 2\ Si\ (g)\ (T > 1763\ K;\ P \sim 1.3\times10^{-4}\ Pa) \quad (9)$$

FactSage™ (CRCT-ThermFact, Inc. and GTT-Technologies) software thermodynamic analyses confirmed the likelihood of the above reaction. While the decomposition of the molten $CrSi_2$ is thermodynamically viable, the fact that partial or nearly complete MI of the preforms was achievable below 1808 K suggests that the process is temperature and time dependent. The remaining charge weight, W_R, was estimated from the empirical Equation (10)

$$W_R = W_0\ (1 - t^n \exp(-Q_v/RT)) \quad (10)$$

where W_0 is the initial weight of the charge, t is the time taken for the charge to attain the MI temperature after it melts[9], Q_v is the activation energy for decomposition, T is the absolute MI temperature, R is the universal gas constant, and n is an adjustable constant.

Figure 15 shows the variation of the W_R against T assuming n = 0.370 and using the experimental value $Q_v/R = 3360$ K for $CrSi_2$ [58]. In calculating W_R, it was assumed that the temperature increased at the rate of 2.5 K/min from the melting point to the MI temperature. The curves shown in Figure 15 are for values of W_0 of 5 and 10 g similar to those used in the present study. The horizontal solid line represents the weight of $CrSi_2$ necessary to fill all the open voids in the preform, which was estimated to be 0.293 g for a typical 10 x 10 x 2.1 mm preform specimen used in the present investigation. For an initial charge of 5 g, these calculations show that there would be insufficient $CrSi_2$ left to infiltrate the preform above 1768 K, whereas a starting charge of 10 g would be insufficient above 1798 K. Thus, the decomposition of $CrSi_2$ appears to be a reasonable explanation for the present observations with the caveat that the Equation (10) is purely empirical. However, there are some inconsistencies in the experimental observations that are difficult to reconcile with this hypothesis. For example, the magnitudes of V_I for two specimens infiltrated at 1778 K were about 20.7 and 0.7% using about 5.5 and 11 g of initial charge, respectively.[10] Similarly, the magnitudes of V_I in two specimens infiltrated at 1803 K for 1800 s were 16.0 and 6.4%, respectively, although the initial charge weights were 3.75 and 13.21 g, respectively.

[9] It is not the MI time.

[10] Although the infiltration times were 3600 and 1800 s, respectively, as noted earlier (Figure 11), the hold time at infiltration temperature did not have any significant effect on the volume fraction of open voids infiltrated.

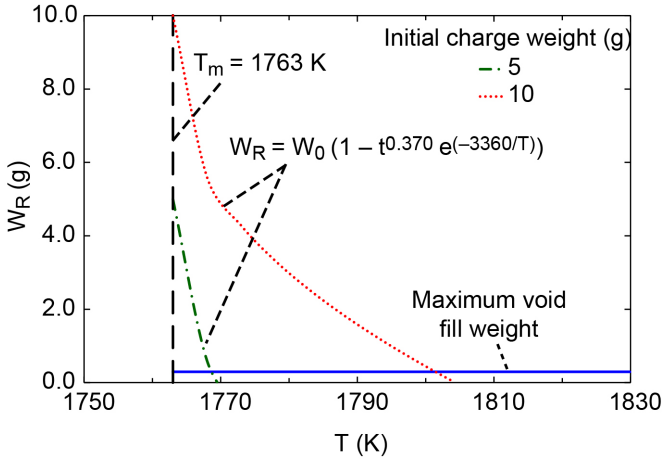

Figure 15.—Predicted remaining charge weight, W_R, against absolute temperature, T, for two initial charge weights. Time, t, represents time required for melt to reach melt infiltration temperature after it reaches melting point, T_m. Solid horizontal line shows weight of charge required to completely fill all open voids in preform.

5.0 Summary and Conclusions

The results of melt infiltrating 2D Tyranno SA3® fiber woven preforms with molten $CrSi_2$ between 1768 and 1896 K for infiltration times between 1800 and 7200 s are reported. It was observed that the maximum volume fraction of infiltrated open voids occurred at 1773 K with the extent of void infiltration decreasing with increasing temperature to 0% above 1805 K independent of the melt infiltration time. Careful microstructural observations revealed that there was no reaction between the SiC_f fibers and the molten $CrSi_2$. Also, Raman spectroscopy was used to confirm that there was no free Si in the infiltrated matrix.

Two possible reasons were examined to explain the decrease in the volume fractions of the infiltrated open voids with increasing temperature above 1773 K. First, the estimated magnitude of the resistance force due to contact angle hysteresis for the molten metal droplets was shown to vary between 0.007 and 0.023 μN. These values are extremely low, and therefore, it is unlikely that a resistance force due to CAH could explain the present observations. Second, the possibility that the $CrSi_2$ charge may have decomposed during heating from the melting temperature to the melt infiltration temperature in the high-vacuum furnace environment was examined. FactSage™ analyses revealed that $CrSi_2$ was likely to dissociate at high temperatures in a high-vacuum environment. Using an empirical equation to describe the amount of remaining charge that is left to infiltrate the preform after it reaches the melt infiltration temperature, it is shown that the present observations could be rationalized for an initial charge of 10 g. While the decomposition of the $CrSi_2$ charge under a high-vacuum environment at high temperatures is a reasonable hypothesis, there were some inconsistencies in the experimental data that could not be rationalized.

References

1. D. Brewer, “HSR/EPM Combustor Materials Development Program,” Mater. Sci. Eng. A, **A261,** (1999), pp. 284-291.
2. H. Ohnabe, S. Masaki, M. Onozuka, K. Miyahara and T. Sasa, “Potential Application of Ceramic Matrix Composites to Aero-Engine Components,” Composites: Part A, **30,** (1999), pp. 489-496.

3. C.M. Grondahl and T. Tsuchiya, "Performance Benefit Assessment of Ceramic Components in a MS9001FA Gas Turbine," J. Eng. Gas Turbine Power, **123,** (2000), pp. 513-519.
4. T. Kameda, Y. Itoh, T. Hishata and T. Okamura, "Development of Continuous Fiber Reinforced Reaction Sintered Silicon Carbide Matrix Composite for Gas Turbine Hot Parts Application," ASME, (2000), p. 2000-GT-67.
5. R.J. Miller, "Design Approaches for High Temperature Composite Aeroengine Components," Comprehensive Composite Materials, **vol. 6**, (2000), pp. 181-207.
6. K.K. Chawla, "Ceramic Matrix Composites" (2nd ed.), Kluwer Academic Publishers, Norwell, MA, 2003.
7. R. Naslain, "Design, Preparation and Properties of Non-Oxide CMCs for Applications in Engines and Nuclear Reactor: An Overview," Comp. Sci. and Tech., **64,** (2004), pp. 155-170.
8. G.S. Corman and K.L. Luthra, "Silicon Melt Infiltrated Ceramic Composites (HiPerComp)," Handbook of Ceramic Composites (edited by N.P. Bansal), Kluwer Academic Publishers, Boston, MA, (2005), pp. 99-115.
9. J.A. DiCarlo, H.M. Yun, G.N. Morscher and R.T. Bhatt, "SiC/SiC Composites for 1200 ºC and Above," Handbook of Ceramics, Glasses and Composites, (edited by N. P. Bansal), Kluwer Academic Publishers, Boston, MA, (2005), pp. 77-98.
10. J.A. DiCarlo and M. van Roode, "Ceramic Composite Development for Gas Turbine Hot Section Components," Proc. GT2006 ASME Turbo Expo 2006: Power for Land, Sea and Air, May 8-11, 2006, Barcelona, Spain.
11. F. Christin, "CMC Materials for Space and Aeronautical Applications," Ceramic Matrix Composites, (edited by W. Krenkel), Wiley-VCH Verlag, (2008), pp. 327-351.
12. M.C. Halbig, M.H. Jaskowiak, J.D. Kiser and D. Zhu, "Evaluation of Ceramic Matrix Composite Technology for Aircraft Turbine Engine Applications". https://ntrs.nasa.gov/archive/nasa/casi.ntrs.nasa.gov/20130010774.pdf, 2013.
13. https://www.researchandmarkets.com/research/m3pjzn/global_ceramic, July 2017.
14. F.W. Zok, "Ceramic-Matrix Composites Enable Revolutionary Gains in Turbine Engine Efficiency," Am. Ceram. Soc. Bull., **95,** (2016), pp. 22-28.
15. G.N. Morscher, "Stress-Dependent Matrix Cracking in 2D Woven SiC-Fiber Reinforced Melt-Infiltrated SiC Matrix Composites," Comp. Sci. Tech., **64,** (2004), pp. 1311-1319.
16. G.N. Morscher, M. Singh, J.D. Kiser, M. Freedman and R. Bhatt, "Modeling Stress-Dependent Matrix Cracking and Stress-Strain Behavior in 2D Woven SiC Fiber Reinforced CVI SiC Composites," Comp. Sci. Tech., **67,** (2007), pp. 1009-1017.
17. G.N. Morscher and V.V. Pujar, "Design Guidelines for In-Plane Mechanical Properties of SiC Fiber-Reinforced Melt-Infiltrated SiC Composites," Int. J. Appl. Ceram. Technol., **6,** (2009), pp. 151-163.
18. G.N. Moscher, "Advanced Woven SiC/SiC Composites for High Temperature Applications," Composites at Lake Louise conference, Oct. 28-Nov. 2 (2007). https://ntrs.nasa.gov/archive/nasa/casi.ntrs.nasa.gov/20080006057.pdf, 2007.
19. S.V. Raj, "Thermal Expansion of Hot-Pressed Engineered Ceramic Materials," Ceram. Intern., **42,** (2016), pp. 2557-2569. http://dx.doi.org/10.1016/j.ceramint.2015.10.058.
20. S.V. Raj, "Development and characterization of hot-pressed matrices for engineered ceramic matrix composites (E-CMCs)," Ceram. Intern., **45,** (2019), pp. 3608-3619. https://doi.org/10.1016/j.ceramint.2018.11.021.
21. S.V. Raj, "High Temperature Creep and Oxidation Resistant Chromium Silicide Matrix Alloy Containing Molybdenum," U.S. Patent No. 5,330,590 issued July 19, 1994.

22. S.V. Raj, "A Preliminary Assessment of the Properties of a Chromium Silicide Alloy for Aerospace Applications," Mater. Sci. Eng. A**, 192-193,** (1995), pp. 583-589.
23. S.V. Raj, "An evaluation of the properties of Cr_3Si alloyed with Mo," Mater. Sci. Eng. A**, 201,** (1995), pp. 229-241.
24. R.M. Dickerson, S.V. Raj and I.E. Locci, "A Preliminary Investigation of the Cr_3Si -Mo Pseudo-Binary Phase Diagram, *Proceedings of the Materials Research Society*, **Vol. 364**, Materials Research Society, Pittsburgh, PA, (1995), pp. 949-954.
25. S.V. Raj, J.D. Whittenberger, B. Zeumer and G. Sauthoff, "Elevated Temperature Deformation of Cr_3Si Alloyed with Mo," Intermetall. **7,** (1999), pp. 743-755.
26. J. Steibel, G.S. Corman, R.C. Schikner and A. Szweda, "Article and Method for Making Complex Shaped Preform and Silicon Carbide Composite by Melt Infiltration," U.S. Patent 6,258,737 B1, July 10, 2001.
27. M. Singh and D.R. Behrendt, "Reactive Melt Infiltration of Silicon-Molybdenum Alloys into Microporous Carbon Preforms," Mater. Sci. Eng. A**, 194,** (1995), pp. 193-200.
28. G.W. Liu, M.L. Muolo, F. Valenza and A. Passerone, "Survey on Wetting of SiC by Molten Metals," Ceram. Intern., **36,** (2010), pp. 1177-1188.
29. A.B. Gokhale and G.J. Abbaschian, *Binary Alloy Phase Diagrams, Vol. 2,* (T.B. Massalski, H. Okamoto, P.R. Subramanian and L. Kacprzak), **Vol. 2**, (1990), pp. 1333-1335.
30. J.A. Champion, B.J. Keene and S. Allen, "Wetting of Refractory Materials by Molten Metallides," J. Mater. Sci., **8,** (1973), pp. 423-426.
31. B. Drevet and Eustathopoulos, "Wetting of Ceramics by Molten Silicon and Silicon Alloys: A Review," J. Mater. Sci., **47,** (2012), pp. 8247-8260.
32. O. Dezellus and N. Eustathopoulos, 'Fundamental Issues of Reactive Wetting by Liquid Metals," J. Mater. Sci., **45,** (2010), pp. 4256-4264.
33. P. Xiao and B. Derby, "Wetting Of Silicon Carbide by Chromium Containing Alloys," Acta Mater., **46** (1998), pp. 3491-3499.
34. S.E. Sheppard, "Relation of Fluidity of Liquids to Temperature," Nature, **125,** (1930), p. 709.
35. J.H. Hildebrand and R.H. Lamoreaux, "Fluidity and Liquid Structure," J. Phys. Chem., **77,** (1973), pp. 1471-1473.
36. L. Makkonen, "A Thermodynamic Model for Contact Angle Hysteresis," J. Chem. Phys., **147,** (2017), p. 064703.
37. G.G. Gnesin and A.I. Raichenko, "Kinetics of Liquid-Phase Reactive Sintering of Silicon Carbide," Sov. Metall. Metal Ceram., **12,** (1973), pp. 383-389.
38. F. Delannay, L. Froyen and A. Deruyttere, "The Wetting of Solids my Molten Metals and its Relation to the Preparation of Metal-Matrix Composites," J. Mater. Sci., **22,** (1987), pp. 1-16.
39. W.B. Hillig, "Melt Infiltration Approach to Ceramic Matrix Composites," J. Am. Ceram. Soc., **71,** (1988), pp. C96-C99.
40. R.P. Messner and Y.M. Chiang, "Liquid-Phase Reaction-Bonding of Silicon Carbide Using Alloyed Silicon-Molybdenum Melts," J. Am. Ceram. Soc., **73,** (1990), pp. 1193-1200.
41. C. Rado, S. Kalogeropoulou and N. Eustathopoulos, "Bonding and Wetting in Non-Reactive Metal/SiC Systems: Weak or Strong Interfaces?," Mater. Sci. Eng. A**, 276,** (2000), pp. 195-202.
42. N. Eustathopoulos, "Wetting by Liquid Metals-Application in Materials Processing: The Contribution of Grenoble Group," Metals, **5,** (2015), pp. 350-370.
43. R.B. Reitz, F.W. Zok and C.G. Levi, "Reactive Alloy Melt Infiltration for SiC Composite Matrices: Mechanistic Insights," J. Am. Ceram. Soc., **100**, (2017), pp. 5471-5481.

44. C.W. Extrand and Y. Kumagai, "An Experimental Study of Contact Angle Hysteresis," J. Colloid Interface Sci., **191**, (1997), pp. 378-383.
45. H.Y. Kim, H.J. Lee and B.H. Kang, "Sliding of Liquid Drops Down an Inclined Solid Surface," J. Colloid Interface Sci., **247**, (2002), pp. 372-380.
46. G. Ahmed, M. Sellier, M. Jermy and M. Taylor, "Modeling the Effects of Contact Angle Hysteresis on the Sliding of Droplets Down Inclined Surfaces," Eur. J. Mech. - B/Fluids, **48**, (2014), pp. 218-230.
47. D. Quéré, M.-J. Azzopardi and L. Delattre, "Drops at Rest on a Tilted Plane," Langmuir, **14**, (1998), pp. 2213-2216.
48. J.F. Joanny and P.G. de Gennes, "A Model for Contact Angle Hysteresis," J. Chem. Phys., **81**, (1984), p. 552-562.
49. L. Gao and T.J. McCarthy, "Contact Angle Hysteresis Explained," Langmuir, **22**, (2006), pp. 6234-6237.
50. E.J. De Souza, L. Gao, T.J. McCarthy, E. Artz and A.J. Crosby, "Effect of Contact Angle Hysteresis on the Measurement of Capillary Forces," Langmuir, **24**, (2008), pp. 1391-1396.
51. H.B. Eral, D.J.C.M.'t Mannetje and J.M. Oh, "Contact Angle Hysteresis: A Review of Fundamentals and Applications," Colloid. Polym. Sci., **291**, (2013), pp. 247–260.
52. M.K. Hubbert, "Darcy's Law and the Field Equations of the Flow of Underground Fluids" Hydrological Sciences Journal, **2**, (1957), pp. 23-59. DOI:10.1080/02626665709493062.
53. C.C. Mei, *Mathematical Analysis in Engineering: How to Use the Basic Tools*, Cambridge University Press (1995). Lecture slides: http://web.mit.edu/fluids-modules/www/porous_media/6-1darcy.pdf.
54. M.R. Sadiq and R. Usha, "Thin Newtonian film flow down a porous inclined plane: Stability analysis," Phys. Fluids, **20**, (2008), pp. 022105:1-22.
55. F. Morrison, *An Introduction to Fluid Mechanics*, Cambridge University Press (2013); Lecture slides: https://pages.mtu.edu/~fmorriso/cm310/selected_lecture_slides.html.
56. M. Sellier and E. Trelluyer, "Modeling the Coalescence of Sessile Droplets," Biomicrofluids, **3**, (2009), p. 022412. https://doi.org/10.1063/1.3154552.
57. K. Persson, Materials Data on $CrSi_2$ by Materials Project (2020), DOI: 10.17188/1188654 https://materialsproject.org/materials/mp-1222/.
58. C.E. Myers, G.A. Murray, R.J. Kematick and M.A. Frisch, "Vaporization Thermodynamics of Chromium Silicides," Report ADR-A162-286, (1985), Office of Naval Research, Arlington, VA.